Mathematical Modeling of Quorum-Sensing Control in Biofilms

John Ward

Abstract This chapter begins with an overview of the relevant literature on theoretical approaches to modeling biofilms, quorum sensing in bacteria, and anti-quorum-sensing treatment. Following this, new mathematical models are proposed to investigate anti-quorum-sensing treatment in batch cultures and in biofilm environments. Details for the models' derivation are aimed so that readers with a nonmathematical background will have a good idea of how such models are constructed and studied. Three anti-quorum-sensing targets are investigated, and a wide variety of outcomes in terms of successful treatment are predicted depending on treatment type, strength, and timing. The many interesting conclusions that can be drawn from the presented results are discussed in detail, including ideas for new experiments, many of which would be considered routine, that will provide deeper insights into how anti-quorum-sensing treatments could be highly effective means of controlling bacterial behavior in a variety of situations and environments.

1 Introduction

The application of mathematics to biology in antiquity was probably little more than a tool to assist in the counting of sheep or cattle. The modeling of population growth seems to have had its beginnings in the Middle Ages, the most famous work being that of Fibonacci of Pisa. In *Liber Abaci*, published in 1202, he derived a formula for rabbit population growth which states that the current population is given by the sum of those of the previous two months, thereby generating his famous eponymous sequence (1, 1, 2, 3, 5, 8, 13, 21, 34, 55, etc.), which essentially amounts to exponential growth. There have, of course, been considerable advancements in the fields

John Ward (✉)
Loughborough University, Department of Mathematical Sciences, Leicestershire, UK,
e-mail: john.ward@lboro.ac.uk

N. Balaban (ed.) *Control of Biofilm Infections by Signal Manipulation*
Springer Series on Biofilms 2
doi: 10.1007/978-3-540-73853-4,

of science, mathematics, and computation since then; however, the basic modeling process is no different from that undertaken by Fibonacci. The aim of mathematical modelers is to formulate a model based on scientifically motivated mechanisms, investigating the resulting system of equations to see whether they can reproduce observations and make new predictions to motivate further experimentation. Ideally, through repeated cycles of model development, validation, and modification, significantly more insight into a problem will be gained than would be possible from experimentation alone. The modeling of quorum-sensing (QS) inhibition therapies in biofilms is in the first such cycle of model development.

Because of their importance in many industrial processes, there has been a long history in biofilm modeling by mathematicians and engineers. Broadly speaking, most mathematical modeling falls into two categories:

1. Continuum models, i.e., models that generate differential equations. See, for example, Atkinson and Davies (1974a,b), Bakke et al. (1984), Dillon et al. (1996), Dockery and Klapper (2001), Freter et al. (1983), and Rittmann and Manem (1992). More examples are discussed below. A pre-1999 review is given in Chaudhry and Beg (1998).
2. Cellular automata, i.e., computational models that use probabilistic "rules" to describe movement and growth from one time-step to the next. See, for example, Eberl et al. (2000), Gonpot et al. (2000), Kreft (2004), Kreft et al. (1998), Noguera et al. (1999), Picioreanu et al. (1998a,b, 2000, 2004), and Wimpenny and Colasanti (1997).

The first approach has the advantage of being more amenable to mathematical analysis and is usually computationally less expensive. In this chapter, a continuum model will be presented that views the biofilm as a multiphase fluid whose growth is principally governed by nutrients that diffuse into the biofilm from the surrounding fluid. This general approach has been adopted by a number of authors investigating single-species biofilm growth (Pritchett and Dockery 2001; Stewart 1994), multispecies biofilm growth (Wanner and Gujer 1986; Wanner and Reichert 1995), growth in porous media (Chen-Charpentier 1999; Tiwari and Bowers 2001), growth in conduits (Szego et al. 1993), the role of the biofilm matrix (Cogan et al. 2005), and antimicrobial resistance (Cogan and Keener 2004).

The mathematical modeling of QS has less history, starting with the near simultaneous publications from three groups, namely James et al. (2000), Dockery and Keener (2001), and Ward et al. (2001). The first two of these papers modeled QS at the molecular level, using the law of mass action to formulate a model consisting of a system of ordinary differential equations. Here, the relevant timescale is in the order of minutes, whereby the population will remain approximately constant and thus act as a parameter in their system. Within appropriate parameter regimes, the authors' analyses showed that there exists a population threshold between very low and very high QS activity. Fagerlind et al. (2003, 2005) extended the work of James et al. (2000) to model the QS system of *Pseudomonas aeruginosa* to study in detail the QS regulatory hierarchy (Fagerlind et al. 2003) and the role of an endogenously produced acyl-homoserine lactone (AHL) antagonist (Fagerlind et al.

2005). Recently, Gorychev et al. (2006) used the same modeling approach to investigate the role of AHL binding with dimeric transcriptional regulators, concluding that dimerization enhances the QS switchlike behavior. Dockery and Keener (2001) and Nilsson et al. (2001) extended these ideas to investigate QS behavior in biofilms, though biofilm growth was not considered in detail. The majority of models have focused on LuxRI homolog systems in gram-negative bacteria, Koerber et al. (2005) used a stochastic modeling approach to describe the QS system employed by the gram-positive *Staphylococcus aureus*. In particular, they studied the role of QS of individual bacteria internalized by nonprofessional phagocytes within endosomes (Hudson et al. 1995), a pathogenic trait that enables bacteria to reproduce within living cells, which is believed to play an important part in prolonging infection.

In the interest of developing a model that can be parametrized using results from routine batch culture experiments, as well as one that can be easily extended to model more complicated situations, Ward et al. (2001) proposed a simple population scale model of QS activity. The timescale of interest is in the order of hours, and the model tracks changes in total population and in subpopulations, the latter reflecting QS activity governed by AHL concentration. The model has relatively few parameters, and data fitting was made possible using results from batch cultures of several strains of *P. aeruginosa*, whereby hourly samples were taken and analyzed to obtain population density and concentrations of the AHLs 3-oxo-C12-homoserine lactone (OdDHL) and *N*-butanoyl-L-homoserine lactone (BHL). The model predicts that the switch from a principally downregulated to an upregulated population occurs very rapidly in comparison to population growth. Ward et al. (2004) extended this model to investigate a range of negative feedback mechanisms known to be involved in QS. A key result was the prediction that a population that would be considered to be QS-active may consist only of a small proportion of upregulated cells at any one time (approximately 5–20%). A simple model for QS in a wound was investigated by Koerber et al. (2002). This model couples the QS model of Ward et al. (2001) with a compartmentalized representation of a wound in which AHL molecules can be lost to the bacteria through diffusion into neighboring regions. Interestingly, the model predicts a rapid jump in QS activity just like that observed in batch cultures, indicating that the QS process is robust even when AHL loss by diffusion is an issue.

Chopp et al. (2002, 2003) and Ward et al. (2003) studied models that coupled biofilm growth and QS, with the aim of identifying key parameters (kinetics, biofilm depth) that govern QS activity. The modeling of biofilms by Chopp et al. is very similar to that described in Sect. 2.2; however, the QS aspects are handled differently. These researchers imposed a critical concentration in their models above which AHL production is massively enhanced; this is not necessary in the model proposed in the next section, as such enhancement of production occurs naturally from the dynamics.

Whereas Chopp et al. (2002, 2003) studied a depth-based model, Ward et al. (2003) modeled biofilms growing over a substratum. The biofilm growth model was not mechanistic (not governed by nutrient concentration) but was chosen so that

the number of parameters is minimal, yet growth can be "made to measure" with regard to how fast the biofilm grows up and along the substratum. This model was coupled with the QS model of Ward et al. (2001) so that the level of AHL buildup within a biofilm can be assessed. This model, and indeed the models of Chopp et al., predict that the shift from low to high QS activity occurs very rapidly throughout the biofilm.

The only publications to date regarding the mathematical modeling of QSIs (as well as antibiotic treatments) are a series of papers by Anguige et al. (2004, 2005, 2006). To explicitly model the effects of furanones (Manefield et al. 1999, 2002; Hentzer et al. 2003) and anti-AHL lactonases (Dong et al. 2002; Lee et al. 2002; Ulrich 2004; Xu et al. 2003), it was necessary to focus on the detailed biochemistry of QS, akin to the approach of James et al. (2000) and Dockery and Keener (2001). The three papers covered the scenarios of batch cultures (Anguige et al. 2004), early biofilm development (Anguige et al. 2005), and mature biofilm development and exopolysaccharide (EPS) production (Anguige et al. 2006). Because of the complexity of these models, the predicted dynamics can be very complex; however, an important result is that the amount of QSI required to be effective in biofilms increases exponentially with biofilm depth. Other key results discussed in these papers will be reproduced by the model studied in this chapter.

In the next section, simplified versions of the mathematical models of Anguige et al. (2004, 2005, 2006) are presented to describe anti-QS treatments in batch cultures and biofilms. This will involve the systematic scale-up from the molecular level to the population level, based on the assumption that the biochemical processes operate on a considerably faster timescale to that of growth. The modeling will consider three QSIs applied to *P. aeruginosa* colonies, namely anti-LasR (e.g., furanones), anti-AHL (e.g., lactonases), and a putative anti-LasI agent. Results from simulations are presented and discussed in the subsequent two sections, and the key points are summarized in the final section.

2 Mathematical Modeling

The anti-QS models developed and studied by Anguige et al. (2004, 2005, 2006) were simplified using the basic ideas of Ward et al. (2001, 2004). The key features of the former studies are maintained, but the new model has fewer parameters, many of which should be determinable using fairly routine experiments.

The model is constructed on the basis of the biochemical pathways involved in the LasRI QS system of *P. aeruginosa*, although it will be applicable to most LuxRI homolog systems. The population of cells (planktonic or sessile) is assumed to consist of two subpopulations:

Downregulated cells. Population density N_{d}. These cells have an empty *lux*-box and, in the case of *P. aeruginosa*, are nonvirulent and produce AHLs and biofilm matrix EPS at a very low background rate.

Upregulated cells. Population density N_u. These cells have a LasR-AHL complex-bound *lux*-box and will express virulent characteristics and produce AHLs and EPS at a significantly enhanced rate.

The total population density is thus $N_T = N_d + N_u$. It is unclear during cell division and chromosomal replication whether a LasR-AHL complex will remain bound to the *lux*-box or not; it will be assumed for simplicity that a downregulated cell will divide into two downregulated cells and that an upregulated cell will divide into one up- and one downregulated cell. The upregulation of downregulated cells is mediated by QS, and downregulation occurs spontaneously (detailed below).

The modeling for QS is based on the work of Ward et al. (2001, 2004); however, because the modeling details are important for the anti-QS therapies, they will be discussed at some length here. Figure 1 shows a schematic LasR/LasI system in *P. aeruginosa* showing the reactions relevant to the modeling. Within all cells it is assumed that LasR (concentration R) is produced at a constitutive rate R_0, binds within a reversible reaction with AHL (A) to form the LasR-AHL complex (P), and

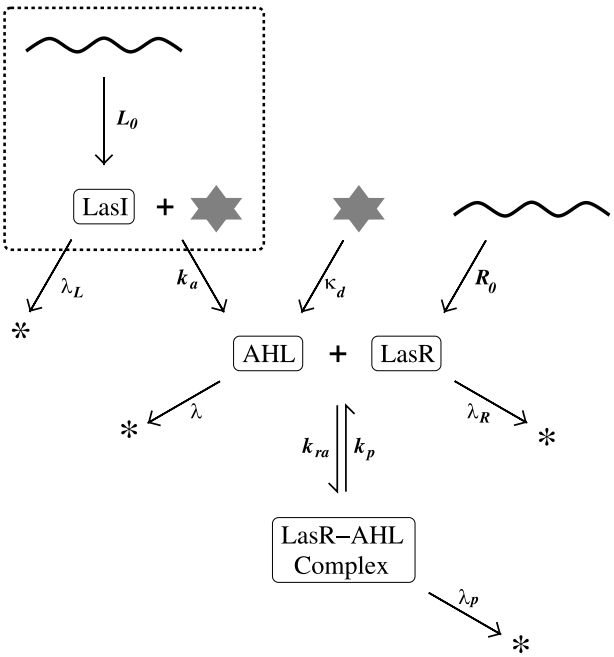

Fig. 1 Schematic of the quorum sensing system LasR/LasI system in *P. aeruginosa* used in the modeling. The figure shows the reactions that are assumed to be occurring in all bacteria, apart from those in the *dashed box* which occur only in the upregulated cells. The *grey stars* represent the reaction between the C_{12}-ACP and *S*-adenosylmethionine that produces the AHL 3-oxo-C12-homoserine lactone (Fuqua and Greenberg 2002), the *wavy lines* represent transcription of the relevant protein and the "*" represent breakdown products. The reaction rate constants for each of the chemical reactions are shown

decays naturally, hence

$$\frac{\mathrm{d}R}{\mathrm{d}t} = R_0 - k_{\mathrm{ra}}AR + k_{\mathrm{p}}P - \lambda_{\mathrm{R}}R\,. \tag{1}$$

The LasR-AHL complex equation is given by

$$\frac{\mathrm{d}P}{\mathrm{d}t} = k_{\mathrm{ra}}AR - k_{\mathrm{p}}P - \lambda_{\mathrm{p}}P\,, \tag{2}$$

in which natural decay of P is also assumed. In upregulated cells, output of LasI occurs at a constant rate and decays naturally according to

$$\frac{\mathrm{d}L}{\mathrm{d}t} = L_0 - \lambda_{\mathrm{L}}L\,. \tag{3}$$

The AHL concentration A represents the measurable AHL concentration in the fluid growth media. Pearson et al. (1999) observed for the AHL 3-oxo-C12-homoserine lactone that the equilibration between internal and external concentrations occurs quickly (in less than 5 min), with internal concentration partitioned to be about three times that of the external. This simply means that $A_{\mathrm{internal}} = \delta A$ (here $\delta \approx 3$) and the relevant parameters below have contained within them this factor δ. AHLs are produced at some background level κ_{d} and decay or become sequestered in fluid with rate constant λ; this, together with the reaction with LasR, yields for downregulated cells

$$\text{the rate of change of AHL in downregulated cells} = \kappa_{\mathrm{d}} - k_{\mathrm{ra}}AR + k_{\mathrm{p}}P - \lambda A\,, \tag{4}$$

and for upregulated cells

$$\text{the rate of change of AHL in upregulated cells} = k_{\mathrm{a}}L + \kappa_{\mathrm{d}} - k_{\mathrm{ra}}AR + k_{\mathrm{p}}P - \lambda A\,, \tag{5}$$

where $k_{\mathrm{a}}L$ describes the massive increase in production of AHLs by upregulated cells. We note that the rate of change of AHL in the external media is simply $-\lambda A$. Compared with cell division time, the timescale adopted in the modeling, these reactions occur very rapidly, and it is reasonable to assume that Eqs. 1–3 are in equilibrium (mathematically, that means $\mathrm{d}R/\mathrm{d}t = \mathrm{d}P/\mathrm{d}t = \mathrm{d}L/\mathrm{d}t = 0$). Hence,

$$L = L_\infty\,, \quad P = \frac{P_\infty}{R_\infty}RA\,, \quad R = \frac{R_\infty}{1+\mu_{\mathrm{R}}A}\,,$$

where $L_\infty = L_0/\lambda_{\mathrm{L}}$, $R_\infty = R_0/\lambda_{\mathrm{R}}$, $P_\infty = R_\infty k_{\mathrm{ra}}/(k_{\mathrm{p}}+\lambda_{\mathrm{p}})$ and $\mu_{\mathrm{R}} = \lambda_{\mathrm{p}}P_\infty/\lambda_{\mathrm{R}}R_\infty$. Fitting the resulting model to experimental data as described in Ward et al. (2004) indicates that $\mu_{\mathrm{R}}A \approx 0$ (i.e., very small), suggesting that most of the LasR is degraded before binding with AHL. For simplicity we will assume that the LasR concentration remains roughly constant at $R = R_\infty$, from which we deduce $P = P_\infty A$. We note that dimerization of R can be modeled in the same way, and it does add a small

amount of complexity to the problem, but the reduction to $R = R_\infty$ will nevertheless result. Substituting these approximations into the AHL production rate equations gives

$$\text{the rate of change of AHL in downregulated cells} = \kappa_\mathrm{d} - \sigma A - \lambda A \tag{6}$$

$$\text{the rate of change of AHL in upregulated cells} = \kappa_\mathrm{u} + \kappa_\mathrm{d} - \sigma A - \lambda A\,, \tag{7}$$

where $\kappa_\mathrm{u} = k_\mathrm{a} L_\infty$ and $\sigma = \lambda_\mathrm{p} P_\infty$. We note in the earlier models (Ward et al. 2001, 2003, 2004; Koerber et al. 2002) that κ_d was absorbed into the κ_u term; however, in order to model the action of the anti-LasI agent explicitly, we shall maintain the terms in their current form. The upregulation rate of cells is assumed to be proportional to the complex concentration $P_\infty A$; letting α_a be the constant of proportionality, then

$$\text{upregulation rate} = \alpha A\,,$$

where $\alpha = \alpha_\mathrm{a} P_\infty$. The downregulation rate of cells is governed by the decay rate of *lux*-bound complexes, which is taken to be β; it is possible that bound complexes have the same degradation properties as their free-floating counterparts, whereby $\beta = \lambda_\mathrm{p}$. Three forms of QSI therapies will be investigated. The first two involve the action of molecules currently being investigated by a number of experimental investigators and discussed by Anguige et al. (2004–2006). The third therapy involves the action of a putative anti-LasI agent.

1. **Anti-LuxR (homolog) agents**, such as halogenated furanones. Using Q_1 to represent the concentration of this agent (to be consistent with the earlier papers), the assumed reaction with LasR can be summarized as follows:

   $$\mathrm{LasR} + Q_1 \xrightarrow{k_1} (1 - \nu_1) Q_1 + \text{by product(s)}\,,$$

   where ν_1 is the average amount of Q_1 lost by the reaction. Using a similar argument to that above, at equilibrium the LasR concentration is given by $R = R_\infty/(1 + \gamma_1 Q_1)$, where $\gamma_1 = k_1/k_\mathrm{R}$. This leads the upregulation rate and the LasR-AHL binding rate to be reduced by a factor of $(1 + \gamma_1 Q_1)$; i.e., the "constants" α and σ now become $\alpha/(1 + \gamma_1 Q_1)$ and $\sigma/(1 + \gamma_1 Q_1)$, respectively.
2. **Anti-AHL agents**, such as lactonases that degrade/quench AHLs. Let Q_2 be the concentration of the lactonase, and then the modeling of lactonase action is based on the simple reaction

   $$\mathrm{AHL} + Q_2 \xrightarrow{\mu_2} (1 - \nu_2) Q_2 + \text{by product(s)}\,,$$

   where ν_2 is the average amount of Q_2 lost by the reaction. This results in an additional "$-\mu_2 Q_2 A$" term in Eqs. 6 and 7.

3. **Anti-LuxI (homolog) agents**, putative to the author's knowledge. Let Q_3 be the concentration of this agent, and then we assume

$$\text{AHL} + Q_3 \xrightarrow{\mu_3} (1-\nu_3)Q_3 + \text{by product(s)}\,,$$

where ν_3 is the average amount of Q_3 lost by the reaction. Similar to the action of Q_1 on LasR, the LasI equilibrium level L_∞ will be reduced to $L_\infty/(1+\gamma_3 Q_3)$ by the agent, where $\gamma_3 = k_3/\lambda_L$. Thus, the AHL output rate term κ_u for upregulated cells now becomes $\kappa_u/(1+\gamma_3 Q_3)$.

All the quantities involved in the modeling are assumed to evolve continuously in time and space, with random stochastic effects neglected. The solutions, therefore, are a prediction of the "average" outcome to be observed experimentally or in situ.

2.1 Anti-QS Treatment in Batch Cultures

The system of equations below is derived from the application of the assumptions given above. For the discussion in the subsequent sections, we will focus on batch culture colony during the exponential phase of growth (doubling time = $\ln(2)/r$), with the drug being introduced either at the start of an experiment or being drip-fed at a rate ϕ_i ($i = 1,2,3$ for Q_1, Q_2, Q_3, respectively). The equations are

$$\frac{\mathrm{d}N_d}{\mathrm{d}t} = rN_T - \frac{\alpha A}{1+\gamma_1 Q_1}N_d + \beta N_u\,, \tag{8}$$

$$\frac{\mathrm{d}N_u}{\mathrm{d}t} = \frac{\alpha A}{1+\gamma_1 Q_1}N_d - \beta N_u\,, \tag{9}$$

$$\frac{\mathrm{d}A}{\mathrm{d}t} = \frac{\kappa_u}{1+\gamma_3 Q_3}N_u + \kappa_d N_T - \frac{\sigma A}{1+\gamma_1 Q_1}N_T - \lambda A - \mu_2 Q_2 A\,, \tag{10}$$

$$\frac{\mathrm{d}Q_1}{\mathrm{d}t} = \phi_1 - \frac{\mu_1 Q_1}{1+\gamma_1 Q_1}N_T - \lambda_1 Q_1\,, \tag{11}$$

$$\frac{\mathrm{d}Q_2}{\mathrm{d}t} = \phi_2 - \mu_2 \nu_2 A Q_2 - \lambda_2 Q_2\,, \tag{12}$$

$$\frac{\mathrm{d}Q_3}{\mathrm{d}t} = \phi_3 - \frac{\mu_3 Q_3}{1+\gamma_3 Q_3}N_u - \lambda_3 Q_3\,, \tag{13}$$

where $N_T = N_u + N_d$. Equations 8–10 in the absence of any drugs are similar to those investigated by Ward et al. (2004), the main difference being that "$\sigma A N_T$" replaces "$A(\alpha N_d + \eta N_T)$" in Eq. 10 and in the absence of the negative feedback term $g(A)$ in Eq. 10. These modifications lead to an adjustment in the best-fit parameters (notably with α and β; see Table 1), but the main results from the mathematical

Table 1 The model parameters and estimated values used in the simulations to follow. The parameters relevant to batch cultures are given above the dividing line, and the additional parameters required for the biofilm are below this line. The values labeled "CS" (current study) are obtained in a semisystematic fashion using best-fit approximation to experimental data (Ward et al. 2004). (For reasons noted in this paper, the best-fit values quoted here are order-of-magnitude approximations and should not be considered as fundamental rate constants.) Figure 2a shows the best-fit solution. L = Lewandowski et al. (1991), S = Stewart (1994), W_1 = Ward et al. (2001), W_2 = Ward et al. (2004), E = estimated value, A = assumed value

Parameter	Units	Description	Value	Source
r	h^{-1}	Cell birth rate	0.5	W_2
α	$\mu M^{-1}\ h^{-1}$	Maximal upregulation rate	9×10^4	CS
β	h^{-1}	Downregulation rate	5.8×10^4	CS
κ_u	$\mu M\ ml\ cell^{-1}\ h^{-1}$	AHL prod. rate by upregulated cells	2.8×10^{-8}	CS
κ_d	$\mu M\ ml\ cell^{-1}\ h^{-1}$	AHL prod. rate by downregulated cells	1.7×10^{-14}	CS[a]
λ	h^{-1}	AHL decay rate	1.5	W_1[b]
σ	$ml\ h^{-1}\ cell^{-1}$	AHL loss rate by LasR/AHL binding	3.8×10^{-8}	CS
μ_1, μ_3	$ml\ h^{-1}\ cell^{-1}$	Drug loss rate due to QSI action	1	A
μ_2	$\mu M^{-1}\ h^{-1}$	Drug loss rate due to QSI action	6×10^5	A
γ_1, γ_3	μM^{-1}	1/conc. when QSI is 50% effective	1.7×10^{-6}	A
ν_1	Dimensionless	Mean Q_2 loss in reaction with AHL	1	A
φ_i	$\mu M\ h^{-1}$	Drip rate of QSI i	varied	–
λ_i	h^{-1}	Decay rate of QSI i	0.06	A[c]
W_0	Dimensionless	Void fraction at maximum bacterial packing	0.3	E
H_0	cm	Initial biofilm depth	0.0002	–
θ	Dimensionless	EPS-generated pore space constant	30	E
ω	Cell/ml biofilm	Maximum density of cells in biofilms	10^{12}	A
κ_E	h^{-1}	Max. EPS prod. rate by upregulated cells	1	A
E_0	h^{-1}	Background EPS production rate	10^{-4}	A
λ_E	h^{-1}	EPS decay rate	0	A[d]
D_a	$cm^2\ h^{-1}$	Diffusion rate of AHL	9×10^{-3}	E[e]
D_i	$cm^2\ h^{-1}$	Diffusion rate of species (Q_i)	9×10^{-3}	$= D_a$
D_c	$cm^2\ h^{-1}$	Diffusion rate of oxygen	9×10^{-2}	S
Q_a	$cm\ h^{-1}$	Surface AHL mass transfer rate	90	A[f]
B_1	h^{-1}	Maximum birth rate	0.1	S
B_2	h^{-1}	Maximum death rate	0.1	E
c_{ext}	μM	Dissolved O_2 concentration	2.3	L
c_1	μM	Half max. birth rate oxygen concentration	0.47	L
c_2	μM	Half max. death rate oxygen concentration	0.47	$= c_1$
τ	Dimensionless	Sets minimum death rate ($= B_2(1 - \tau)$)	1	E
ρ	μM	Oxygen consumption constant	4×10^5	L

[a] too small to be estimated reliably; [b] measurement in bovine serum; [c] 10 hour half life; [d] assumed negligible in the timescale of interest; [e] assumed $1/10^{th}$ that of oxygen; [f] biofilms are assumed to readily leak AHLs into the environment, hence a large Q_a/D_a is imposed

analysis described in the earlier work are entirely relevant to the current model. The parameters yet to be defined are the rate constants $\mu_1 = \nu_1 k_1$ and $\mu_3 = \nu_3 k_3$.

Figure 2a shows that the best-fit solutions of Eqs. 8–10 are in good agreement with experimentally measured AHL concentrations; the parameter values are listed in Table 1. The data were obtained from a batch culture experiment during the expo-

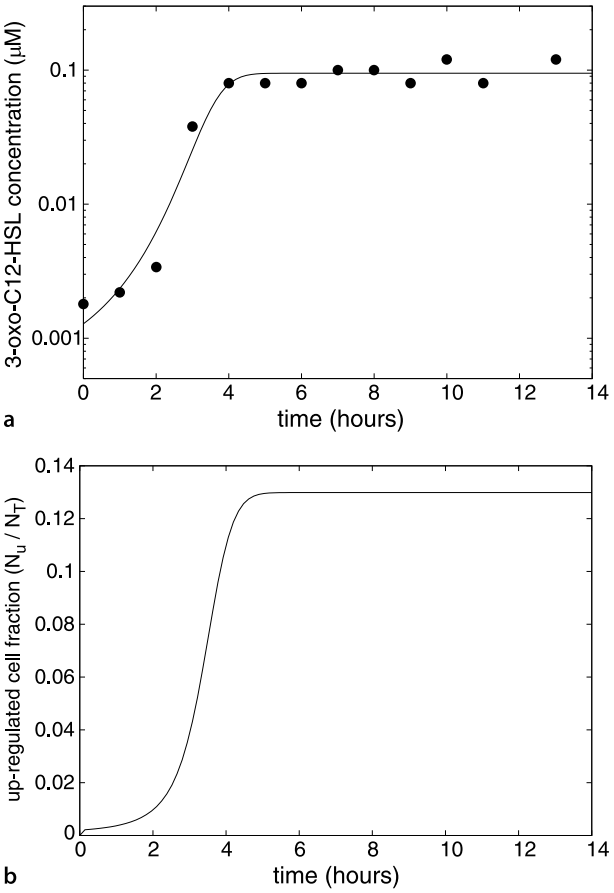

Fig. 2 Plot **a** shows the evolution of 3-oxo-C12-HSL concentration against time in an exponentially growing bacterial colony in a batch culture; the *solid line* is the solution of the model equations (8)–(10) using the parameters in Table 1, and "•" indicate the experimental values. Plot **b** depicts the fraction of upregulated cells for the same simulation

nential growing phase of *P. aeruginosa* strain PAB1 (a clinical burn wound isolate). Full details of the experimental work are given in Ward et al. (2001, 2004).

2.2 Anti-QS Treatment in Biofilms

To model biofilms it is necessary to consider bacterial cell distributions as functions of time t and space z, where z is the "perpendicular" distance from the base of the biofilm such that the biofilm surface is located at $z = H(t)$. Here, the bacterial subpopulations N_{u} and N_{d} are to be viewed as volume fractions, so that the volume

fraction of living cells is $N_u + N_d = N_T$. Through continued nutrient deprivation, cells die and occupy a volume fraction M; it is assumed that dead cells remain intact for the timescale of interest (a few days). The remaining space in the biofilm is occupied EPS (volume fraction E) and water (volume fraction W), hence $N_T + M + E + W = 1$. In the report by Anguige et al. (2006), it was further assumed that as EPS is produced, the resulting pore space increases proportionately, thus entraining more water, i.e., $W = W_0 + \theta E$ for constants W_0 and θ (in Anguige et al. 2006, α is used instead of θ). This leads to the condition

$$N_T + M + (1+\theta)E = 1 - W_0 \,, \tag{14}$$

where $1 - W_0$ is the maximum fraction of space that cells occupy. For example, if cells are spherical, then, according to Kepler's conjecture (or perhaps more familiarly, the "grocer's orange-stacking problem"), $W_0 \approx 0.26$ (Sloane 1998). Biofilm growth is assumed to be governed by the QS-regulated EPS production and nutrient concentration c (entering the biofilm by diffusion through the surface); although the relevant parameters regarding nutrients are based on oxygen, the modeling can be used to consider any nutrient. The local changes in volume by cell division, death, and EPS production cause movement within the biofilm; this process is called advection, and the speed of movement is described by velocity v. The growth rate of the biofilm surface is thus given by the surface value of v. The QS process is modeled in exactly the same way as that of the batch culture described above. The AHL, QSIs, and nutrient are assumed to be diffusible compounds, and all, apart from the anti-AHL agent Q_2, can enter and leave cells in such a way that the internal and external concentrations equilibrate rapidly (in a few minutes) compared to the biofilm growth timescale (hours). After a little simplification in the same manner as that described by Anguige et al. (2006), the system of equations is as follows:

$$\frac{\partial N_T}{\partial t} + \frac{\partial v N_T}{\partial z} = N_T(F_b(c) - F_d(c)) \,, \tag{15}$$

$$\frac{\partial M}{\partial t} + \frac{\partial v M}{\partial z} = N_T F_d(c) \,, \tag{16}$$

$$\frac{\partial N_u}{\partial t} + \frac{\partial v N_u}{\partial z} = \frac{\alpha A}{1+\gamma_1 Q_1} N_d - \beta N_u \,, \tag{17}$$

$$\frac{\partial E}{\partial t} + \frac{\partial v E}{\partial z} = (E_0 N_T + \kappa_E N_u) F_b(c) - \lambda_E E \,, \tag{18}$$

$$0 = D_a \frac{\partial^2 A}{\partial z^2} + \frac{\kappa_u^*}{1+\gamma_3 Q_3} N_u + \kappa_d^* N_T - \frac{\sigma^* A}{1+\gamma_1 Q_1} N_T - \lambda A - \mu_2 Q_2 A \,, \tag{19}$$

$$0 = D_1 \frac{\partial^2 Q_1}{\partial z^2} - \frac{\mu_1^* Q_1}{1+\gamma_1 Q_1} N_T - \lambda_1 Q_1 \,, \tag{20}$$

$$0 = D_2 \frac{\partial}{\partial z}\left(W \frac{\partial Q_2}{\partial z}\right) - \mu_2 \nu_2 A W Q_2 - \lambda_2 W Q_2 \,, \tag{21}$$

$$0 = D_3 \frac{\partial^2 Q_3}{\partial z^2} - \frac{\mu_3^* Q_3}{1+\gamma_3 Q_3} N_\mathrm{u} - \lambda_3 Q_3 \,, \tag{22}$$

$$0 = D_\mathrm{c} \frac{\partial^2 c}{\partial z^2} - \rho N_\mathrm{T} F_\mathrm{b}(c) \,, \tag{23}$$

$$\frac{\partial v}{\partial z} = \frac{1}{1-W_0}\left(N_\mathrm{T} F_\mathrm{b}(c) + (1+\theta)(E_0 N_\mathrm{T} + \kappa_\mathrm{E} N_\mathrm{u}) F_\mathrm{b}(c) - \lambda_\mathrm{E} E\right) \,, \tag{24}$$

$$\frac{\mathrm{d}H}{\mathrm{d}t} = v(H,t) \,. \tag{25}$$

Here, functions F_b and F_d are the birth and death rates of living cells, respectively, so the cell growth rate is simply the difference between the two functions in Eq. 15. Equation 16 states that living cells die at a rate $F_\mathrm{d} N_\mathrm{T}$, although M can be eliminated from the system using Eq. 14 since $M = 1 - W_0 - N_\mathrm{T} - (1+\theta)E$. The right-hand side of Eq. 17 is the same as Eq. 9, where the volume fraction of downregulated cells can be obtained from $N_\mathrm{d} = N_\mathrm{T} - N_\mathrm{u}$. Equation 18 states that the EPS is produced at a background level by all living cells (at rate $E_0 N_\mathrm{T} F_\mathrm{b}$), but the production rate is significantly enhanced by upregulated cells ($k_\mathrm{E} N_\mathrm{u} F_\mathrm{b}$). Equations 10–13 become Eqs. 19–22 to account for diffusion; for simplicity we have assumed the quasisteady (no time derivatives) form of these and the nutrient (Eq. 23) equations, due to as is generally the case, the fact that the chemical diffusion processes are rapid in comparison to growth. Because the anti-AHL concentration within the water is Q_2, the overall concentration is thus WQ_2 (recalling $W = W_0 + \theta E$), hence Eq. 21 results. The constants labeled with * are modified versions of the batch culture case due to the change of definition from cell density to cell fraction, so that $\kappa_\mathrm{u}^* = \omega \kappa_\mathrm{u}$, where ω is the maximum number of cells per millileter of biofilm (approximately 10^{12} cells/ml^{-1}); constants κ_d^*, σ^*, μ_1^* and μ_3^* are similarly redefined. Equation 24 is derived by summing Eqs. 15, 26, and $\theta\times$ Eq. 18 and applying Eq. 14. The last equation states that the speed of the biofilm surface moves at the same velocity as the cells on the surface. The functions $F_\mathrm{b}(c)$ and $F_\mathrm{d}(c)$ are bacterial cell birth and death rates, respectively, as functions of c; typically, the birth rate increases and the death rate decreases as the nutrient increases. In the simulations to follow, Michaelis-Menten (or monod)-type kinetics are used, namely

$$F_\mathrm{b}(c) = B_1 \frac{c}{c_1 + c} \,, \quad F_\mathrm{d}(c) = B_2\left(1 - \tau \frac{c}{c_2 + c}\right) \,.$$

The rate of cell birth is assumed to reflect the amount of general activity a cell is undertaking; hence, EPS production and nutrient consumption are assumed to be proportional to $F_\mathrm{b}(c)$. Equations 15–25 require a set of initial boundary conditions to be fully specified. The simulations are assumed to start shortly after the first few bacteria have settled onto a substrate. There are no upregulated cells or EPS. The

following are imposed:

$$
\begin{aligned}
&t = 0 \qquad N_{\mathrm{T}} = 1 - W_0\,, \quad N_{\mathrm{u}} = 0\,, \quad E = 0\,, \quad H = H_0 \\
&z = 0 \qquad \frac{\partial A}{\partial z} = 0\,, \quad \frac{\partial c}{\partial z} = 0\,, \quad \frac{\partial Q_1}{\partial z} = 0\,, \quad \frac{\partial Q_2}{\partial z} = 0\,, \quad \frac{\partial Q_3}{\partial z} = 0\,, \quad v = 0 \\
&z = H(t) \quad c = c_{\mathrm{ext}}\,, \quad D_{\mathrm{a}} \frac{\partial A}{\partial z} = -Q_{\mathrm{a}} A\,.
\end{aligned}
$$

The conditions at $x = 0$ are no flux conditions; that is, no material is allowed to cross $x = 0$. The nutrient concentration is assumed to be of fixed concentration c_{ext} (oxygen dissolved in water at saturated levels is imposed), and the condition on AHL means that the flux of AHL out of the biofilm is proportional to the difference of internal A and external (assumed zero) concentrations.

We note that the model described here is one-dimensional, with growth occurring perpendicular to a solid surface. We therefore do not intend to describe the elaborate spatial structures (water channels, mushrooms) that are often observed in experimental studies (Hentzer et al. 2001). Describing these features requires a significant development of the modeling specifically, the fluid-dynamic aspects, which are beyond the scope of the current study. Furthermore, no mechanisms are included in the model that will lead to growth limitations, such as planktonic cell escape or sloughing of biofilm material due to the effect of shear forces on its surface from the fluid media. However, the current model should describe fairly well the first few days of development, during which time most experimental studies are undertaken.

In the next two sections, simulations of the models described above are presented to investigate the effect of the three types of QSIs on the QS process. In the absence of specific data, particularly with regard to drug kinetics, the simulations are aimed at presenting the key qualitative results that might be expected in experiments, along with their implications for effective treatment for biofilms. We will first consider the batch culture case and how QSI potency and dosage affect upregulation. For biofilms, this too will be considered together with the key issues of treatment timing and drug delivery via diffusion.

3 Anti-QS Therapies in Batch Cultures

Figure 2 shows a typical time evolution of AHL concentration and upregulated cell fraction ($N_{\mathrm{u}}^{\mathrm{frac}}$, given by $N_{\mathrm{u}}^{\mathrm{frac}} = N_{\mathrm{u}}/N_{\mathrm{T}}$) for an exponentially growing population in an untreated batch culture. Figure 2b demonstrates the key characteristic feature of QS. After an initial period in which very little upregulation occurs, there is very rapid upregulation (here, at around 3 h), whereby a maximally upregulated population is reached. It is worth noting that the concept of "critical AHL concentration" is not included in the model, and such a phenotypic shift is in fact due to the basic dynamics of the QS system at a molecular level. However, a fascinating prediction by the model is that only a portion of cells in an "upregulated" population will be

upregulated (here, about 12–13%) at any time. The model predicts this because there is a balance between AHL molecule production and upregulation rates against AHL loss by unused LasR-AHL complex formation and by spontaneous downregulation by upregulated cells.

The key mechanisms involved in upregulating bacteria in batch cultures are dependent on the growth phase. Using the mathematical methods described by Ward et al. (2001, 2004), it can be shown that to get substantial upregulation in a LuxR-LuxI homolog QS system, the parameter values must satisfy the following:

$$\text{exponential growth phase:} \quad \Theta = \alpha\kappa_{\mathrm{u}} - \sigma(\beta + r) > 0 \tag{26}$$

$$\text{stationary phase:} \quad \Psi = \alpha\kappa_{\mathrm{u}} K - \beta(\sigma K + \lambda) > 0\,, \tag{27}$$

where K is the total population density at the stationary phase. The parameters to the left of the "$-$" sign are concerned with the mechanisms that promote QS, while those to the right are inhibiting mechanisms. Thus, Θ and Ψ are formulations representing the balance between the positive and negative QS mechanisms for each of the two growth phases. Using the data in Table 1, we have $\Theta \approx 3 \times 10^{-3}$ and $\Psi \approx 3 \times 10^{6}$ (assuming a stationary phase density of 10^{10} cells/ml), both being positive, meaning that substantial upregulation is expected. Using the same mathematical methods, when $\Theta > 0$ and $\Psi > 0$, the fraction of upregulated cells $N_{\mathrm{u}}^{\mathrm{frac}}$ in a quorate population can be calculated:

$$\text{exponential growth phase:} \quad N_{\mathrm{u}}^{\mathrm{frac}} = 1 - \frac{\sigma(\beta + r)}{\alpha\kappa_{\mathrm{u}}}\,,$$

$$\text{stationary phase:} \quad N_{\mathrm{u}}^{\mathrm{frac}} = 1 - \frac{\beta(\sigma K + \lambda)}{\alpha\kappa_{\mathrm{u}} K}\,.$$

Given appropriate data, we can use these formulas to estimate how virulent a bacterial colony can be. Furthermore, they make explicit how targeting a parameter, using a putative QSI, will restrict QS and perhaps prevent expression of virulence characteristics.

In the next two subsections, solutions to the model equations are discussed for the cases in which the the QSI is administered by drip-feeding or by pretreatment of the growth media. The former case is perhaps more relevant to anti-QS treatment of biofilms discussed in Sect. 4, in which diffusion acts as a "feeding" mechanism to cells deep within the colony.

3.1 Drip-Feed Administration of QSI

Figure 3 shows the steady-state AHL concentration and upregulated cell fraction against population size K for an untreated culture 3a and for cultures drip-fed with QSIs 3b–d. Because very little data are currently available regarding the dynamics of the QSIs, the parameters were chosen so that the rapid jump in Fig. 3b and the

right-most fold in Fig. 3c and d occur at about the same population density (approximately 2×10^{10} cells/ml). In the absence of treatment, Fig. 3a shows that increasing K leads to a smooth increase in upregulated cell fraction, rising very sharply (at $K = K_{\text{jump}} \approx 2\times10^{8}\,\text{cells}/\text{ml}$), beyond which a maximal level is reached (approximately 12–13% of cells). In contrast to the predictions of the modeling of Dockery and Keener (2000), the current model does not predict a hysteresis response; this is due to the assumption here that LasR production is not upregulated by QS (see Anguige et al. 2004).

Figure 3b–d demonstrates the range of results that can occur with the anti-AHL treatments. Anti-LasR agents lead to results that are qualitatively similar to those of the no-treatment case, while AHL and LasI blocking agents can lead to a hysteresis response. The rather unexpected hump around 10^{10} cells/ml in the left graph of Fig. 3b is due to there being less LasR present to soak up the AHLs, leading to greater accumulation; with increasing population, the anti-LasR agents become less effective, so AHL levels decrease to those of the no-treatment case. Two rather bold observations can be made from these figures with regard to effectiveness of QSI:

1. Direct comparison of the potency of the QSI can be meaningfully made only between the anti-LasR and anti-LasI, due to these having similar kinetic terms. Of particular interest, given that the rate constants are same, is that the drip-feed rate of the anti-LasI agent is 100 times less than that of the anti-LasR agent, suggesting that an anti-LasI agent will, by a considerable margin, be the more effective of the two treatments.
2. In practice, application of QSIs will be combined with antibiotics, and hysteresis is an unfavorable property for effective treatment. For the cases shown in Fig. 3c and d, an established quorate population will require more antibiotic drug to force the population density to levels below the left-hand folds in the curves. In this respect, anti-LasR treatment seems likely to be the most effective QSI.

Of course, these observations are based on a particular parameter set, and any conclusions must be treated with some caution. However, they highlight the need for experimental data to determine the parameters involved so that assertions such as these can be made with more confidence.

The evolution of upregulated cell fraction is shown in Fig. 4, in which the effects of each QSI can be compared with the untreated case. Here the population density is growing exponentially, starting with a density of 10^{7} cells/ml. As expected, each treatment delays the onset of substantial upregulation, but in these simulations they will not prevent substantial upregulation as the exponentially growing population will eventually exceed the critical densities depicted in Fig. 3. However, as would be expected in practice, the limitations on attainable population density mean that sufficient drug will totally inhibit QS in batch cultures. The contrast in qualitative behaviors between the agents is interesting. For both the anti-LasR and anti-AHL cases, there is a rapid jump in cell fraction at about $t = 18\,\text{h}$, roughly corresponding to the time when the population density reaches the critical level; the hump in the anti-LasR case is due to a brief overshoot in AHL concentration resulting from

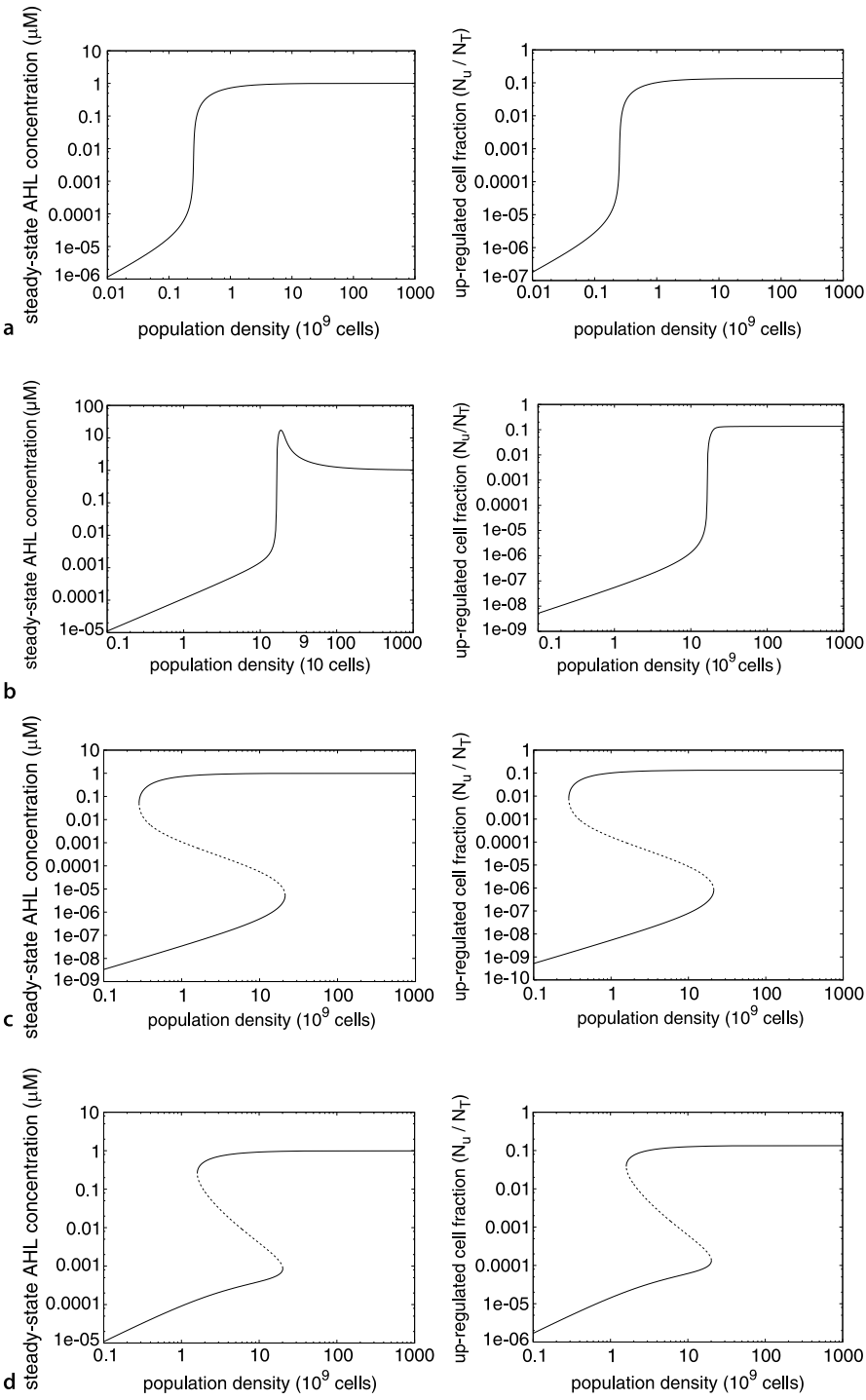
a
steady-state AHL concentration (μM)
population density (10^9 cells)
up-regulated cell fraction (N_u / N_T)
population density (10^9 cells)
b
steady-state AHL concentration (μM)
population density (10 cells)
up-regulated cell fraction (N_u/N_T)
population density (10^9 cells)
c
steady-state AHL concentration (μM)
population density (10^9 cells)
up-regulated cell fraction (N_u / N_T)
population density (10^9 cells)
d
steady-state AHL concentration (μM)
population density (10^9 cells)
up-regulated cell fraction (N_u / N_T)
population density (10^9 cells)

◄ **Fig. 3** Log-log plots showing the steady-state 3-oxo-C12-HSL concentration (*left*) and upregulated cell fraction (*right*) as functions of the population density for **a** untreated cultures, **b** with anti-LuxR agent (with $\varphi_1 = 3.3 \times 10^{-3}$ μM/h), **c** anti-AHL agent ($\varphi_2 = 5 \times 10^{-3}$ μM/h) and **d** anti-LuxI agent ($\varphi_3 = 3.3 \times 10^{-5}$ μM/h). Figures **c** and **d** exhibit hysteresis, the *solid* and *dashed curves* indicating the stable and unstable solutions respectively. The remaining parameters are given in Table 1

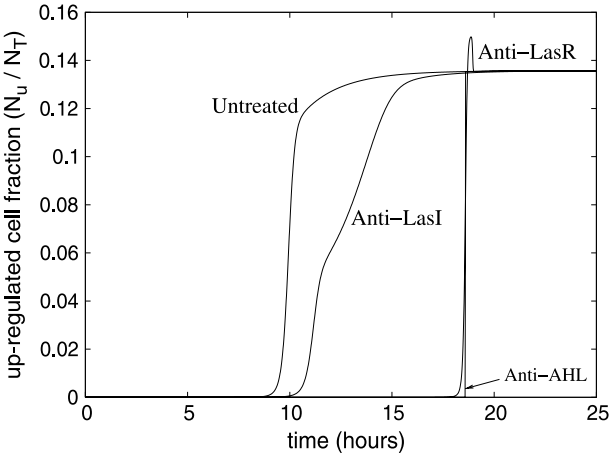

Fig. 4 Evolution of the upregulated cell fraction against time for exponentially growing bacterial colonies for untreated and drip-fed treated cultures (drip-feed rates were the same as those used in Fig. 3). In this simulation, the anti-AHL and anti-LasR cases are superimposed. The remaining parameters are given in Table 1

less available LasR at this point to soak up the AHLs. The gradual rise of upregulation in the anti-LasI case is a result of the relatively low drip-feed rate, leading to considerably less agent being present at the critical time when the population becomes quorate. However, this is very sensitive to the drip-feed rate; for example, doubling the rate to $\phi_3 = 6.6 \times 10^{-5}$ requires the population density to reach unphysical levels (approximately 2×10^{13}) before a jump to quorate levels can occur (not shown).

3.2 Quorum Sensing in Pretreated Media

Probably the simplest way to investigate the effects of QSIs on QS is to grow batch cultures in pretreated growth media. Figure 5 shows a simulation of such an experiment, with the initial agent concentration chosen so that the colony becomes quorate at around the same time (note that the drip-feed component of the model has been "switched off", i.e., $\phi_i = 0$). The time interval required to sufficiently consume the QSI as the population grows leads to a delay in the onset of extensive upregulation, as expected. The anti-LasI agent compares well against the anti-LasR agent in that

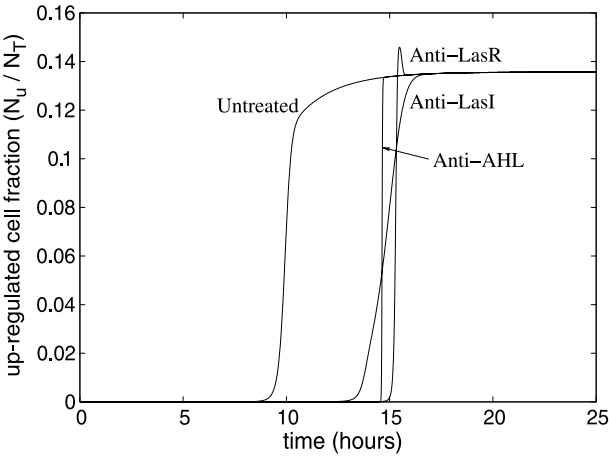

Fig. 5 Evolution of the upregulated cell fraction against time for exponentially growing bacterial colonies for an untreated culture and cultures grown in pretreated media. The initial concentrations of the anti-LasR, anti-AHL, and anti-LasI agents are $1.7 \times 10^{-2}\,\mu$M, $1.7 \times 10^{-2}\,\mu$M, and $5 \times 10^{-5}\,\mu$M, respectively. The remaining parameters are given in Table 1

significantly less agent was initially required to produce similar results (recall that the equivalent kinetic rate constants are the same for each).

Figure 6 shows the effects of the initial QSI concentration on the timescale for substantial upregulation. As expected, low concentrations of the agent have minimal impact, and the concentration needs to be above a certain threshold before the effects are noticeable. Interestingly, the curves for anti-LasR and anti-AHL are

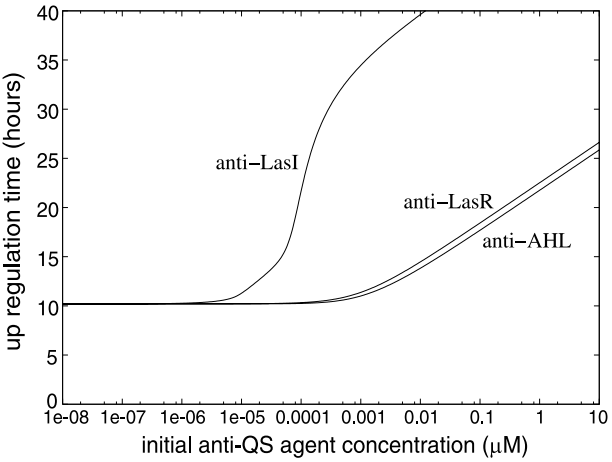

Fig. 6 The effects of the initial QSI concentration on the timescale for substantial upregulation (taken to be when $N_u/N_T = 10\%$) for batch culture colonies grown in pretreated media. The remaining parameters are given in Table 1

qualitatively similar; we note that the quantitative similarity is an accident of parameter choice. Noting that the horizontal scale is logged, the model predicts that beyond the concentration threshold of anti-LasR or anti-AHL agent, the timescale increases in a logarithmic fashion; this means that a substantial increase in agent is required to effect a noticeable delay in upregulation. Once again, the anti-LasI agent has apparently outperformed the other two agents by inducing considerable delays in upregulation at much lower concentrations. We note that in these simulations the population density is increasing exponentially and the stationary phase of growth has not been accounted for; if the agent succeeds in suppressing QS upregulation into the stationary phase, then the timescales shown in Fig. 6 will be pessimistic lower bound.

4 Anti-QS Therapies in Biofilms

Results from a typical simulation of growth of an untreated biofilm are shown in Figs. 7 and 8. The vast majority of experimental results discussed in the literature tend to be qualitative rather than quantitative in terms of biofilm growth, so accurate estimation of the parameters concerning growth is not possible. The parameters for the simulations were chosen so that the biofilm grows at a rate of approximately 6 μm/h, with a thickness of around 450 μm after 100 h, which seems reasonable given various experimental data. The model predicts that after an initial acceleration of growth, because of all bacterial cells being adequately nourished and undergoing cell division, the biofilm growth rate will slow down, eventually growing linearly in time without limitation (Fig. 7a,b). Of course, it is not possible for biofilms to grow indefinitely, but, as stated above, the aim is to have a good description of growth in the first few days of development. The linear growth phase results from nutrient diffusion limitations, in which only cells within a certain, eventually fixed, distance from the surface will have adequate nutrients to divide and produce EPS; cells deeper in the biofilm will be nonreproductive or dead. The assumption that EPS production is regulated by QS leads, as expected, to the significantly enhanced growth rate of the simulated wild-type over the QS-ve strain, in qualitative agreement with the experimental observations of Davies et al. (1998). This will have a significant effect on the delivery of the QSIs (discussed below) and, indeed, antibiotics (see Anguige et al. 2005, 2006). Plots of growth rate against time give a good indication of the timescale and extent of upregulation within the biofilms, and they will be used to illustrate the efficacy of the QSIs.

The advance toward high levels of QS activity is illustrated in Fig. 7c and d. For the first 26 h, AHL levels increase but remain relatively low [(see panels (a) and (b)]; thus, the growth rates between wild-type and QS-ve strains are indistinguishable. However, within a time interval of 1 h, there is a substantial rise in AHL levels (approximately 10000-fold increase), leading to rapid upregulation (see Fig. 6d) and divergence between the growth rates as the EPS production rate by wild-type cells is greatly enhanced. Here, the total upregulated cell fraction $U(t)$ is defined

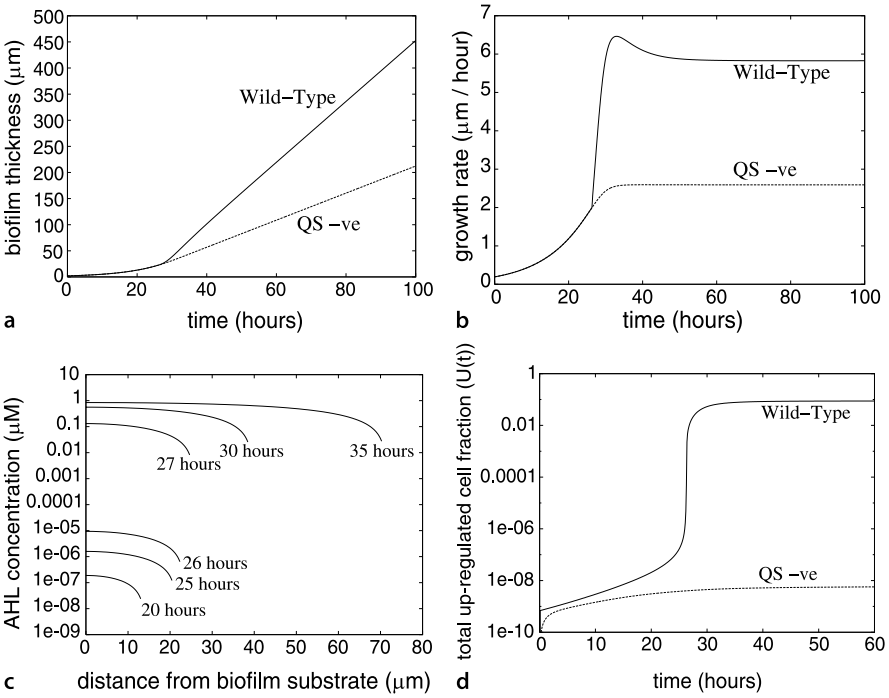

Fig. 7 Selected plots of simulated growth of an untreated biofilm. Comparison of the evolution of biofilm depth (**a**) and biofilm growth rate (**b**) for a wild-type and a QS-ve strain. Quorum sensing activity of the wild-type strain is demonstrated using AHL distribution at various time intervals up to 35 h (**c**) and the total upregulated cell fraction against time (**d**). Parameter values are given in Table 1

mathematically to be

$$U(t) = \frac{\int_0^{\mathrm{H}} N_{\mathrm{u}}(z,t)\mathrm{d}z}{\int_0^{\mathrm{H}} N_{\mathrm{T}}(z,t)\mathrm{d}z},$$

which can be viewed as the mean upregulated fraction divided by the mean live cell fraction over the entire the biofilm. Soon after, the spatial structure of the biofilm settles to the profiles indicated in Fig. 8, which move along as the biofilm grows. The overshoot in growth rate of the wild-type cells around $t = 30$ is due to the slow death rate of anoxic cells. In time, these cells die, reducing the depth at which EPS is produced and leading to a marginal slowing down of growth.

The distributions of living cells, upregulated cells, EPS, and water after 100 h are shown in Fig. 8c. The living cells are located in a region near the surface, corresponding to an area where there is a nonnegligible concentration of nutrients. The biofilm structure mainly consists of water (about 70%), and EPS occupies a volume percentage of 3%, which is in broad agreement with observations in fairly mature biofilms (Boyle et al. 1999). Because the dynamics are such that in optimum con-

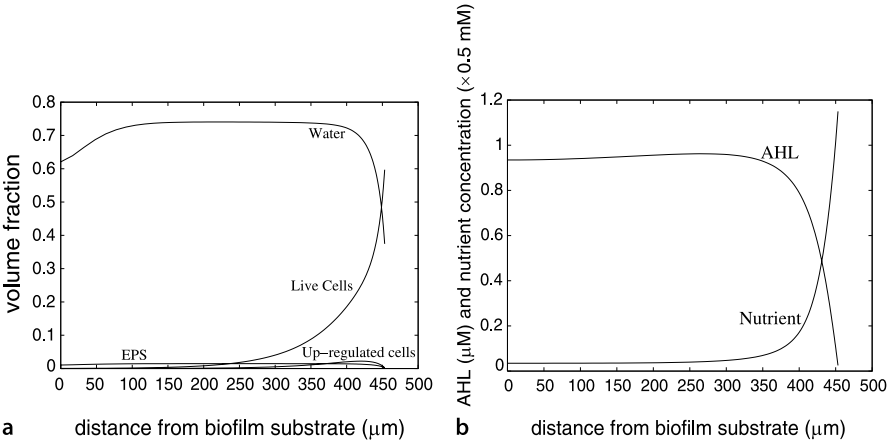

Fig. 8 Spatial distribution of live cell, EPS, water, and upregulated cell fractions (**a**) and AHL and nutrient concentration (**b**) at $t = 100$ h for an untreated wild-type biofilm. Parameter values are given in Table 1

ditions only 10% of cells will be upregulated, the upregulated cell fraction remains fairly low; however, this may still represent a population that is significantly virulent. The AHL distribution shown in Fig. 8b is elevated deep in the biofilm, dropping off sharply toward the edge because of the relatively high mass transfer rate compared with diffusion at the surface. The drop in live cell fraction moving deeper into the biofilm is paralleled by the drop in nutrient concentration (Fig. 8b), whereby much of the biofilm is predicted to be anoxic within a few days.

In the simulations to follow, the effectiveness of QSI will mostly be assessed by comparing the growth rate (i.e., $\mathrm{d}H/\mathrm{d}t$) of a treated biofilm with those of the wild-type and QS-ve strains, since EPS production and the enhanced growth it generates are markers for QS activity. The treatment will be presumed effective if the growth rate is reduced to that of the QS-ve strain, reflecting very low levels of QS activity, virulence, and EPS production.

4.1 Biofilm Growth in Media Pretreated with QSIs

Figure 9 shows the evolution of the growth rates and total upregulated cell fraction for biofilms grown in media containing a fixed concentration of QSI. Interestingly, for all treatments the shift in growth rates from the maximal to the minimal levels occur within an order of magnitude (on the μM scale) of drug concentration and is particularly sharp in the anti-AHL case.

Qualitatively, the results of the anti-LasR and anti-LasI agents are similar, there being a smooth transition down to the minimal growth rate as the drug concentration increases. For intermediate agent levels, the outer cells mostly remain downregu-

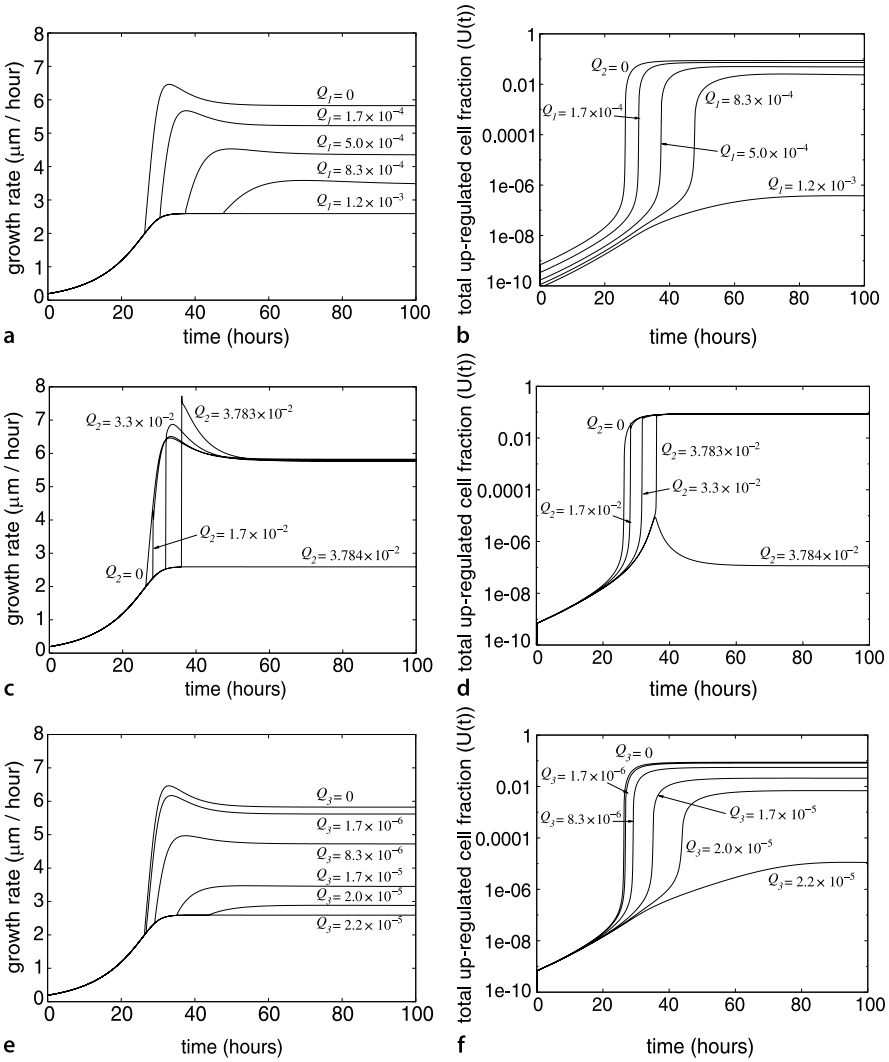

Fig. 9 The effects of applied concentrations (values in μM) of anti-LuxR (**a** and **b**), anti-AHL (**c** and **d**), and anti-LasI (**e** and **f**) agents on biofilm growth. Figures **a**, **c**, and **e** show the biofilm growth rate, and **b**, **d**, and **f** show the upregulated cell fraction (N_u/N_T) against time up to $t = 100$. Parameter values are given in Table 1

lated but prevent sufficient agent penetration to those cells deeper in the biofilm. As observed before, significantly less anti-LasI agent is required in the media to produce the desired effect. In terms of virulence (Fig. 9b,f), it can be observed that even when the agent has significantly reduced the speed of growth, the fraction of upregulated cells is considerably higher than the minimal levels (Fig. 7d), so a number of cells express virulent characteristics that could be significant in a clinical setting.

In contrast, increasing anti-AHL agent concentration makes little difference in long-term biofilm development until a threshold is reached (here, about 3.783×10^{-2} μM). The existence of the sharp transition, typical of systems with underlying hysteresis in the dynamics as described in Sect. 3, is due to the nature of the agent's target. Anti-AHL agents do not prevent production of AHLs, as these will always be produced at a background level and diffuse throughout the biofilm. The penetration of the anti-AHL agent, however, is limited by both diffusion and AHL reaction in the living cell region of the biofilm. Consequently, if insufficient anti-AHL agents reach the regions deep within the biofilm, the AHLs will accumulate there, forming a reservoir that will supply the living cells, eventually reaching a critical level that will induce mass upregulation of cells. The resulting AHL output will be sufficient to swamp the incoming anti-AHLs so that their effect will be negligible. We note that the concept of "critical concentration" of AHLs is not straightforward; the critical level of AHLs in biofilms will also depend on the bacterial growth rate, nutrient diffusion, and consumption rate, i.e., a host of parameters not directly related to QS dynamics. It is also clear from Fig. 9d that the anti-AHL agent must be above the threshold to have any effect on the eventual level of upregulation and, hence, on virulent behavior.

4.2 Growth Response to Delayed Application of QSIs

To investigate whether a more mature biofilm will have greater resistance to anti-AHLs than a nascent one, the biofilm was simulated to grow untreated for 36 h before the QSI was applied. Figure 10 illustrates the main results.

As before, for the anti-LasR and anti-LasI agents (Fig. 10a,c), the outcomes are similar; here, the concentrations used are exactly those that *just* brought about minimal growth in the pretreated media case. Both agents induced a rapid decline in growth, eventually settling to the minimal growth rate (the fact that the curves appear identical is coincidental). The sharp jump is due to the assumed fast dynamics of the biochemical processes. In the anti-LasR case (Fig. 10a), the agent will diffuse in rapidly, resulting in a near immediate shutdown of upregulation throughout, so the upregulated cells that spontaneously downregulated are not replaced. For the set of parameters used, the concentration $Q_1(H,t) = 1.2\times10^{-3}$ will always reduce growth to the minimal level. The results for the anti-LasI case (Fig. 10c) are surprising because it would be expected that when the agent is applied, the LasI present in the upregulated cells near the surface would, for a period, be sufficient to limit the agent's effect deeper into the biofilm. Although this is probably true in many situations, here the parameters are such that the processes of LasI removal, spontaneous downregulation of upregulated cells, and downturn in AHL production happen very rapidly, leading to the dramatic drop in biofilm growth rate. The results suggest that these drugs can be applied at any time and that the growth rate will be reduced accordingly. Of course, the biofilm with the delayed treatment has had a head start and will be thicker than a pretreated biofilm (Fig. 10d). This may be significant with

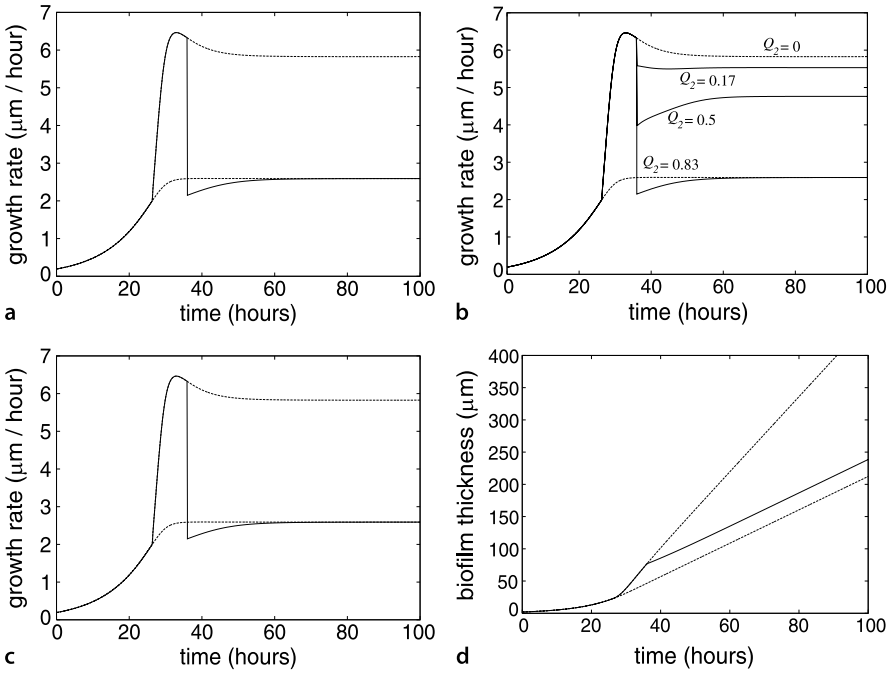

Fig. 10 The effects of a delayed application (36 h) of QSIs on the biofilm growth rate (Figs. **a**–**c**) and biofilm depth (Fig. **d**); the *dashed lines* are the corresponding curves for untreated wild-type and QS-ve bacteria (same as those shown in Fig. 7a and b). Figure **a** shows the effects of the anti-LasR agent ($Q_1(H,t) = 1.2 \times 10^{-3}$ μM), **b** anti-AHL (external concentrations as shown in μM) and **c** and **d** are the results for the anti-LasI agent ($Q_3(H,t) = 2.2 \times 10^{-5}$ μM). The *dashed curves* in **d** shows the growth rate of the wild-type (*upper*) and QS-ve strain (*lower*) and the treated biofilm is shown by the *solid line*. Parameter values are given in Table 1

regard to antibiotic penetration when a combined therapy is used; however, at the very least, the bacteria should not be virulent.

For the anti-AHL agent, a thicker biofilm has enormous implications (Fig. 10b). In these simulations, the concentration needed to induce a notable effect on the growth rate is over 10 times that for the pretreated case. This is to be expected, as after 36 h the level of upregulation is such that AHL production is at near-full capacity; consequently, there is ample AHL present to soak up the drug near the surface before it penetrates deep into the biofilm. Unlike the pretreated case, there is no longer a threshold concentration, the growth rate declining steadily as the agent increases.

4.3 Role of QSI Diffusion

One of the key issues in delivering a drug to a site of action involves its diffusive properties. Broadly speaking, larger molecules diffuse more slowly, so more of the

drug will need to be administered for it to reach the target areas. The effects of the QSI diffusion coefficient on biofilm growth rate and total upregulated cell fraction are shown in Fig. 11; only anti-LasR and anti-AHL simulations are shown because the anti-LasI produced results similar to the former agent. In the simulations up to now, the diffusion coefficients of AHL and QSIs have been assumed to be the same, which would be expected if the molecular masses are roughly the same (the molecular mass of 3-oxo-C12-HSL being 297).

Figure 11a and b shows the results of biofilm development in pretreated media containing an anti-LasR concentration of 1.7×10^{-3} μM, well within the range that would restrict biofilm growth to minimal levels given a drug diffusion of $D_1 = 9\times10^{-3}\,\mathrm{cm^2\,h^{-1}}$. As expected, the reduced drug penetration that results from decreasing the diffusion coefficient enhances biofilm growth and upregulation.

Interestingly, within the physical ranges of the diffusion coefficient D_2, the critical concentrations of anti-AHL agent in pretreated media varied very little (results not shown); for example, reducing the diffusion coefficient 100 times to

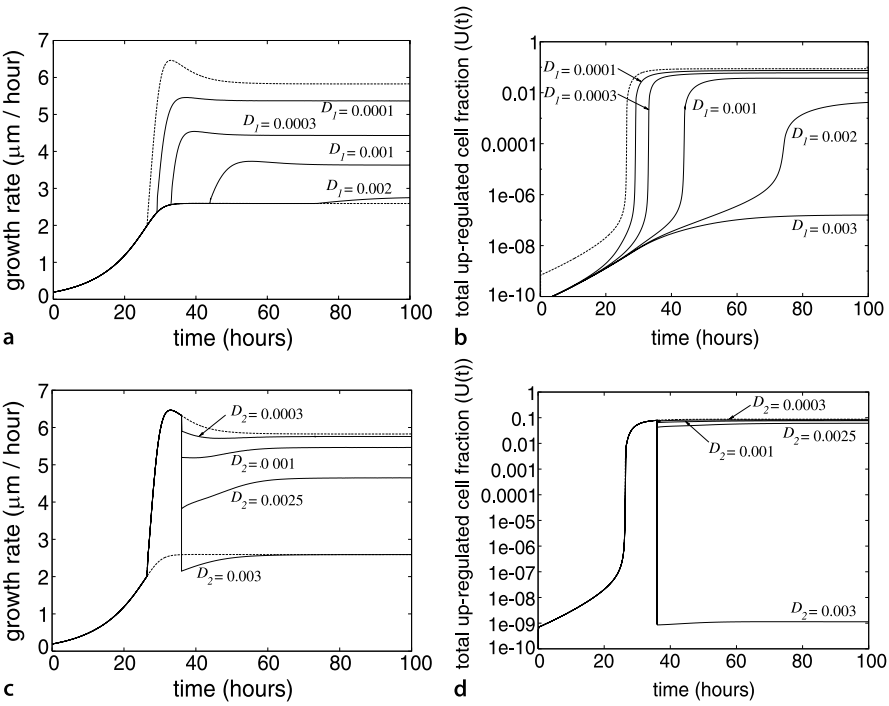

Fig. 11 The effects of the QSI diffusion coefficient (values shown have units $\mathrm{cm^2\,h^{-1}}$) on the evolution of the biofilm growth rate and upregulated cell fraction. Parts **a** and **b** show growth in media containing a fixed anti-LasR concentration $Q_1(H,t) = 1.7 \times 10^{-3}$ μM, and **c** and **d** shows the response to a 36-h delayed application of anti-AHL agent, at concentration $Q_2(H,t) = 1.7$ μM. The *dashed curves* are the results from the untreated wild-type and QS-mutant. Parameter values are given in Table 1

$D_2 = 9 \times 10^{-5}\,\mathrm{cm}^2\,\mathrm{h}^{-1}$ increases the critical concentration by less than 10%. This is mainly due to the anti-AHLs being present in the biofilm from the start of growth, so the transport properties of the agent are not crucial in preventing AHL accumulation. However, it is a different story when the agent is administered to a mature biofilm. Figure 11c and d shows the results of a very high anti-AHL dose (1.7 μM) administered at 36 h. Here, relatively small changes to the diffusion coefficient can have a significant effect on the outcome of biofilm development and in particular the level of upregulation that occurs (Fig. 11d). This again illustrates the underlying hysteresis in the dynamics of anti-AHL agents.

5 Concluding Remarks and Scope for Further Experimentation

The mathematical modeling described here and by Anguige et al. (2004, 2005, 2006) are the first attempts at modeling the effects of anti-QS therapies on bacteria growth, biofilm development, and virulence. These models incorporate biologically and physically relevant mechanisms and, in the absence of data, produce results that seem reasonable. Despite the current paucity of quantitative data regarding QSIs, through simulation and mathematical analysis a number of qualitative predictions and assertions can be made from the modeling:

1. In both batch cultures and biofilms, early application of a sufficient amount of QSI will delay or prevent the onset of mass upregulation. In a clinical setting, delaying QS and virulence is perhaps all that is needed for an agent to be useful, as this could buy sufficient time for the immune system to respond effectively and for an infected wound to heal normally.
2. During the exponential phases of growth in both batch cultures and biofilms, the amount of QSI required to suppress QS increases exponentially. This is illustrated for the anti-AHL and anti-LasR agents in Fig. 6 and has been shown (mathematically) by Anguige (2005) to be the case for biofilms. If dosing levels of an anti-AHL drug are an issue, then early application would be essential.
3. The dynamics of anti-AHL and anti-LasI agents have an underlying hysteresis. It is possible that once a population is upregulated, a considerable amount of agent will be needed to force downregulation. This again stresses the need for early application of QSIs, ideally prior to the onset of substantial upregulation. If hysteresis dynamics are observed experimentally for the anti-LasR agent, then it is likely that LasR is upregulated by QS (Anguige 2004); the models will need to be modified accordingly.
4. For biofilms, the range of concentrations of applied QSI that separate minimal and maximal QS suppression seems to be quite narrow, particularly in the anti-AHL case. Furthermore,when the growth rate is even slightly above the minimal level, the fraction of upregulated cells present is many times greater than that for a fully QS-suppressed colony; virulence expression in the biofilm could well be significant in such circumstances.

5. The simulations consistently suggest that the putative anti-LasI treatment seems to be the most potent one for suppressing QS. Of course, this is very much dependent on the parameter values, but its effectiveness is due largely to the fact that when few upregulated cells are present, there is very little LasI present to soak up the agent.
   Given the lack of relevant experimental data regarding anti-AHL and anti-LasR, it is difficult to make bold conclusions as to their relative merits based on results from the mathematical models. Typically, there will be considerably less LasR in the system than AHL, so less anti-LasR would be required. However, the anti-LasR must be able to get inside the cell, which may be a significant restriction in a practical setting.

Some of these qualitative predictions should be experimentally verifiable, the results of which would provide a means of validating the models and continuing the mathematical modeling cycle referred to in the introduction of this chapter.

To make quantitative, rather than qualitative, predictions and conclusions from the mathematical models, good quantitative experimental data are needed. Even with the addition of QSIs in the current model, there are only a handful of parameters to be fitted. Some of these parameters, such as the diffusion and decay rates of QSI, should be determinable from nonculture experiments. The remaining parameters can be obtained using data from batch cultures grown in media that are treated and untreated with QSIs; hourly measurements of population density, AHL concentration, and QSI concentration can be fitted to the model in the manner described by Ward et al. (2001). Such experiments will assist enormously in the development of the current mathematical model so that they can be more predictive and capable of offering further insights into the action of anti-QS treatments.

References

Anguige K, King JR, Ward JP, Williams P (2004) Mathematical modeling of therapies targeted at bacterial quorum sensing. Math Biosci 192:39–83

Anguige K, King JR, Ward JP, Williams P (2005) Modeling antibiotic- and anti-quorum sensing treatment of a *Pseudomonas aeruginosa* biofilm. J Math Biol 51:557–594

Anguige K, King JR, Ward JP (2006) A multi-phase mathematical model of quorum sensing in a maturing *Pseudomonas aeruginosa* biofilm. Math Biosci 203:240–276

Atkinson B, Davies IJ (1974a) The overall rate of substrate uptake (reaction) by microbial film. Part I – a biological rate equation. Trans Inst Chem Eng 52:260–268

Atkinson B, Davies IJ (1974b) The overall rate of substrate uptake (reaction) by microbial film. Part II – effect of concentration and thickness with mixed microbial films. Trans Inst Chem Eng 52:248–259

Bakke R, Trulear MG, Robinson JA, Characklis WG (1984) Activity of *Pseudomonas aeruginosa* in biofilms: steady state. Biotech and Bioeng 26:1418–1424

Boyle JD, Dodds I, Lappin-Scott H, Stoodley P (1999) Limits to growth and what keeps a biofilm finite. Anitmicrobial Agents Chemo 38:303–315

Chaudhry MAS, Beg SA (1998) A review on the mathematical modeling of biofilm processes: advances in fundamentals of biofilm modeling. Chem Eng Technol 21:701–710

Chopp DL, Kirisits MJ, Moran B, Parsek MR (2002) A mathematical model of quorum sensing in a growing bacterial biofilm. J Indust Microbiol Biotech 29:339–346

Chopp DL, Kirisits MJ, Moran B, Parsek MR (2003) The dependence of quorum sensing on the depth of a growing biofilm. Bull Math Biol 65:1053–1079

Cogan NG, Cortez R, Fauci L (2005) Modeling physiological resistance in bacterial biofilms. Bull Math Biol 67:831–853

Cogan NG, Keener JP (2004) The role of the biofilm matrix in structural development. Math Med Biol 21:147–166

Davies DG, Parsek MR, Pearson JP, Iglewski BH, Costerton JW, Greenberg EP (1998) The involvement of cell-to-cell signals in the development of a bacterial biofilm. Science 280:295–297

Dockery JD, Keener JP (2001) A mathematical model for quorum sensing in *Pseudomonas aeruginosa*. Bull Math Biol 63:95–116

Dockery J, Klapper I (2001) Finger formation in biofilms layers. SIAM J Appl Math 62:853–869

Dillon R, Fauci L, Fogelson A, Gaver D III (1996) Modeling biofilm processes using the immersed boundary method. J Comp Phys 129:57–73

Dong YH, Gusti AR, Zhang Q, Xu JL, Zhang LH (2002) Identification of quorum-quenching *N*-acyl homoserine lactonases from *Bacillus* species. Appl Environ Microbiol 68:1754–1759

Eberl HJ, Picioreanu C, Heijnen JJ, van Loosdrecht MCM (2000) A three-dimensional numerical study on the correlation of spatial structure, hydrodynamic conditions, and mass transfer and conversion in biofilms. Chem Eng Sci 55:6209–6222

Fagerlind MG, Nilsson P, Harlén M, Karlsson S, Rice SA, Kjelleberg S (2005) Modeling the effect of acylated homoserine lactone antagonists in *Pseudomonas aeruginosa*. Biosystems 80:201–213

Fagerlind MG, Rice SA, Nilsson P, Harlén M, James S, Charlton T, Kjelleberg S (2003) The Role of Regulators in the Expression of Quorum-Sensing Signals in *Pseudomonas aeruginosa*. J Mol Microbiol Biotechnol 6:88–100

Freter R, Brickner H, Fekete J, Vickerman M, Carey K (1983) Survival and implantation of *Escherichia coli* in the intestinal tract. Infect Immun 39:686–703

Fuqua C, Greenberg EP (2002) Listening in on bacteria: acyl-homosering lactone signalling. Mol Cell Biol 3:685–695

Gonpot P, Smith R, Richter A (2000) Diffusion limited biofilm growth. Mod Simul Mater Sci Eng 8:707–726

Goryachev AB, Toh DJ, Lee T (2006) Systems analysis of a quorum sensing network: design constraints imposed by the functional requirements, network topology and kinetic constants. Biosystems 83:178–187

Hentzer M, Teitzel GM, Balzer GJ, Heydorn A, Molin S, Givskov M, Parsek MR (2001) Alginate overproduction affects *Pseudomonas aeruginosa* biofilm structure and function. J Bacteriol 183:5395–5401

Hentzer M, Wu H, Andersen JB, Riedel KB, Rasmussen T, Bagge N, Kumar N, Schembri MA, Song Z, Kristoffersen P, Manefield M, Costerton JW, Molin S, Eberl L, Steinberg P, Kjelleberg S, Hoiby N, Givskov M (2003) Attenuation of *Pseudomonas aeruginosa* virulence by quorum sensing inhibitors. EMBO J 22:3803–3815

Hudson MC, Ramp WK, Nicholson NC, Williams AS, Nousiainen MT (1995) Internalisation of *Staphylococcus aureus* by cultured osteoblasts. Microb Pathog 19:409–419

James S, Nilsson P, James G, Kjelleberg S, Fagerstrøm T (2000) Luminescence control in the marine bacterium *Vibrio fischeri*: an analysis of the dynamics of *lux* regulation. J Mol Biol 296:1127–1137

Koerber AJ, King JR, Ward JP, Williams P, Croft JM, Sockett RE (2002) A mathematical model of partial-thickness burn-wound infection by *Pseudomonas aeruginosa*: quorum sensing and the build-up to invasion. Bull Math Biol 64:239–259

Koerber AJ, King JR, Williams P (2005) Deterministic and stochastic modeling of endosome escape by *Staphylococcus aureus*: "quorum" sensing by a sungle bacterium. J Math Biol 50:440–488

Kreft JU (2004) Biofilms promote altruism. Microbiology 150:2751–2760

Kreft JU, Booth G, Wimpenny JWT (1998) BacSim, a simulator for individual-based modeling of bacterial colony growth. Microbiology 144:3275–3287

Lee S, Park S, Lee J, Yum D, Koo B, Lee J-K (2002) Genes encoding the *N*-Acyl Homoserine Lactone-Degrading Enzyme Are Widespread in Many Subspecies of *Bacillus thuringiensis*. Appl Environ Microbiol 68:3919–3924

Lewandowski Z, Walser G, Characklis WG (1991) Reaction Kinetics in Biofilms. Biotech and Bioeng 38:877–882

Manefield M, De Nys R, Kumar N, Read R, Givskov M, Steinberg P, Kjelleberg S (1999) Evidence that halogenated furanones from *Dlisea pulchra* inhibit acylated homoserine lactone (AHL)-mediated gene expression by displacing the AHL signal from its receptor protein. Microbiology 145:283–291

Manefield M, Rasmussen TB, Hentzer M, Andersen JB, Steinberg P, Kjelleberg S, Givskov M (2002) Halogenated furanones inhibit quorum sensing through accelerated LuxR turnover. Microbiology 148:1119–1127

Nilsson P, Olofsson A, Fagerlind MG, Fagerstrøm T, Rice S, Kjelleberg S, Steinberg P (2001) Kinetics of the AHL regulatory system in a model biofilm system: how many bacteria constitute a "quorum". J Mol Biol 309:631–640

Noguera DR, Pizarro G, Stahl DA, Rittmann BE (1999) Simulation of multispecies biofilm development in three dimensions. Wat Sci Tech 39:123–130

Pearson JP, van Dalden C, Iglewski BH (1999) Active efflux and diffusion are involved in transport of *Pseudomonas aeruginosa* cell-to-cell signals. J Bacteriol 181:1203–1210

Picioreanu C, Kreft JU, van Loosdrecht MCM (2004) Particle-based multidimensional multispecies biofilm model. Appl Environ Microbiol 70:3024–3040

Picioreanu C, van Loosdrecht MCM, Heijnen JJ (1998a) A new combined differential-discrete cellular automaton approach for biofilm modeling: application for growth in gel beads. Biotech and Bioeng 57:718–731

Picioreanu C, van Loosdrecht MCM, Heijnen JJ (1998b) Mathematical modeling of biofilm structure with a hybrid differential-discrete cellular automaton approach. Biotech and Bioeng 58:101–116

Picioreanu C, van Loosdrecht MCM, Heijnen JJ (2000) Effect of diffusive and convective substrate transport on biofilm structure formation: a two-dimensional modeling study. Biotech and Bioeng 69:504–515

Pritchett LA, Dockery J (2001) Steady state solutions of a one-dimensional biofilm model. Math Comput Model 33:255–263

Rittmann BE, Manem JA (1992) Development and experimental evaluation of a steady-state, multispecies biofilm model. Biotech Bioeng 39:914–922

Sloane NJA (1998) Kepler's conjecture confirmed. Nature 395:435–436

Stewart PS (1994) Biofilm accumulation model that predicts antibiotic resistance of *Pseudomonas aeruginosa* biofilms. Anitmicrobial Agents Chemo 38:1052–1058

Szego S, Cinnella P, Cunningham AB (1993) Numerical simulation of biofilm growth in closed conduits. J Comp Phys 108:246–263

Tiwari SK, Bowers KL (2001) Modeling biofilm growth and porous media applications. Math Comput Model 33:299–319

Ulrich RL (2004) Quorum quenching:enzymatic disruption of *N*-acylhomoserine lactone-mediated bacterial communication in *Burkholderia thailandensis*. Appl Environ Microbiol 70:6173–6180

Viretta AU, Fusseneggar M (2004) Modeling the quorum sensing regulatory network of human-pathogenic *Pseudomonas aeruginosa*. Biotechnol Prog 20:670–678

Wanner O, Gujer W (1986) A Multispecies Biofilm Model. Biotech and Bioeng 28:314–328

Wanner O, Reichert P (1995) Mathematical modeling of mixed culture biofilms. Biotech and Bioeng 49:172–184

Ward JP, King JR, Koerber AJ, Croft JM, Sockett RE, Williams P (2003) Early development and quorum sensing in bacterial biofilms. J Math Biol 47:23–55

Ward JP, King JR, Koerber AJ, Williams P, Croft JM, Sockett RE (2004) Cell-signalling repression in bacterial quorum sensing. Math Med Biol 21:169–204

Ward JP, King JR, Koerber AJ, Williams P, Croft JM, Sockett RE (2001) Mathematical modeling of quorum sensing in bacteria. IMA J Math Appl Med Biol 18:263–292

Wimpenny JWT, Colasanti R (1997) A unifying hypothesis for the structure of microbial biofilms based on cellular automaton models. FEMS Microbiol Ecol 22:1–16

Xu F, Byun T, Dussen HJ, Duke KR (2003) Degradation of *N*-acylhomoserine lactones, the bacterial quorum-sensing molecules, by acylase. Biotechnology 101:89–96